Journal of Alloys and Compounds 509 (2011) 5368–5372

Contents lists available at ScienceDirect

Journal of Alloys and Compounds

journal homepage: www.elsevier.com/locate/jallcom

Iron fluorides assisted dehydrogenation and hydrogenation of MgH_2 studied by Mössbauer spectroscopy

I.E. Malka [a], A. Błachowski [b], K. Ruebenbauer [b,*], J. Przewoźnik [c], J. Żukrowski [c], T. Czujko [a], J. Bystrzycki [a]

[a] Department of Advanced Materials and Technologies, Military University of Technology, PL-00-908 Warsaw, ul. S. Kaliskiego 2, Poland
[b] Mössbauer Spectroscopy Division, Institute of Physics, Pedagogical University, PL-30-084 Cracow, ul. Podchorążych 2, Poland
[c] Solid State Department, Faculty of Physics and Applied Computer Science, AGH University of Science and Technology, PL-30-059 Cracow, Al. Mickiewicza 30, Poland

ARTICLE INFO

Article history:
Received 26 January 2011
Accepted 9 February 2011
Available online 15 February 2011

PACS:
88.30.rd
76.80.+y

Keywords:
Hydrogen storage
MgH_2
Mg_2FeH_6
Mössbauer spectroscopy

ABSTRACT

Mechanically milled MgH_2 with the addition of 7 wt.% of either FeF_2 or FeF_3 were investigated by means of the X-ray powder diffraction and Mössbauer spectroscopy as prepared and upon dehydrogenation and finally upon subsequent hydrogenation. Mechanical milling leads to the decomposition of iron fluorides. In the case of FeF_2 one obtains magnesium solid solution in metallic BCC iron as the dominant iron-bearing phase, while for FeF_3 one gets Mg_2FeH_6 as dominant phase with iron. Dehydrogenation at 325 °C leads to removing defects and formation of magnesium, iron and $MgH_{2-x}F_x$ phases for both types of dopants, i.e., FeF_2 and FeF_3. Subsequent hydrogenation at 325 °C leaves β-MgH_2 as a major phase. However, for original material doped with FeF_3 one has iron predominantly in the Mg_2FeH_6 compound, while for FeF_2 dopant iron occurs mostly as nearly pure BCC metallic phase. Mössbauer spectra indicate that Mg_2FeH_6 does not order magnetically down to 4.2 K.

1. Introduction

Magnesium could be used as convenient material for hydrogen storage. However, hydrogenation and dehydrogenation rates of pure magnesium are too slow in temperature range compatible with working temperature of proton exchange membrane (PEM) fuel cell. It has been shown that addition of transition metal halides (or halides of other metals showing strong catalytic effects) reduces significantly temperature of efficient hydrogen desorption. Particularly 3d metal fluorides seem to have the large effect [1–5]. Dehydrogenation of the milled material starts at about 30 °C lower temperature with addition of FeF_2 in comparison with addition of FeF_3 [4]. Similar results have been obtained by Jin et al. [3]. They have shown that dehydrogenation of the MgH_2 milled with FeF_2 starts below 300 °C. Synthesis of ternary hydride Mg_2FeH_6 during milling of above material has been observed as well [3].

The present contribution reports on preparation of the material made by mechanical milling of MgH_2 and 7 wt.% of either FeF_2 or FeF_3. Subsequently, the material was dehydrogenated and hydrogenated again. X-ray diffraction patterns as well as Mössbauer spectra applying 14.41-k eV transition in ^{57}Fe were obtained after each of above steps. Mössbauer spectroscopy is useful to trace iron chemical states in various phases provided iron is used as above mentioned 3d metal.

2. Experimental

Commercial powder of MgH_2 (AlfaAesar, 99.8% purity) with 7 wt.% of either FeF_2 or FeF_3 (Sigma–Aldrich, 98% purity) were mechanically milled using Fritsch P6 planetary mill for one hour under high purity argon (99.999% purity, H_2O and O_2 below 1 p.p.m. each). The total mass of each sample amounted to 5 g. All samples were loaded with thirty 10-mm diameter stainless steel balls into 80-ml vial of stainless steel. The ball to powder mass ratio was about 25, and the vial was rotated at 650 r.p.m. Starting materials and powders after milling were stored under argon atmosphere with oxygen and water vapor content below 0.1 p.p.m. each. Dehydrogenation was carried out at 325 °C for 10 min under 1 bar pressure of hydrogen. Subsequent hydrogenation was performed at the same temperature and for the same time interval under 10-bar pressure of hydrogen (99.9999% purity).

Powder X-ray diffraction patterns were obtained at room temperature by using D5000 Siemens diffractometer. The Cu-Kα1,2 radiation was used with the pyrolitic graphite monochromator on the detector side. The scans were performed for $2\theta = 10 - 110°$ with the step 0.03°. Data were analyzed by the Rietveld method as implemented in the FULLPROF program.

* Corresponding author. Tel.: +48 12 662 6317; fax: +48 12 637 2243.
E-mail address: sfrueben@cyf-kr.edu.pl (K. Ruebenbauer).

0925-8388/$ – see front matter © 2011 Elsevier B.V. All rights reserved.
doi:10.1016/j.jallcom.2011.02.049

Table 1A
Results obtained by the X-ray powder diffraction method. Symbol C stands for the contribution of the respective phase, symbols *a*, *b* and *c* denote lattice constants, where applicable. Marks (a)–(c) represent results for the FeF_2 doped material upon milling, dehydrogenation and hydrogenation, respectively. Marks (d)–(f) show corresponding results for the FeF_3 doped material.

	C (wt.%)	*a*, *b* (Å)	*c* (Å)		C (wt.%)	*a*, *b* (Å)	*c* (Å)
(a) – FeF_2 doped: milled				(d) – FeF_3 doped: milled			
β-MgH_2	65(5)	4.512(4)	3.017(3)	β-MgH_2	80(2)	4.511(4)	3.020(3)
γ-MgH_2	20(3)	4.60(5)	5.03(4)	γ-MgH_2	18(1)	4.54(3)	4.97(2)
		5.28(3)				5.34(2)	
Fe(Mg)	15(2)	2.96(1)		Mg_2FeH_6	2(1)	6.47(1)	
(b) – dehydrogenated				(e) – dehydrogenated			
Mg	85(5)	3.212(1)	5.215(2)	Mg	86(2)	3.211(1)	5.214(1)
$MgH_{2-x}F_x$	4(1)	4.55(2)	3.04(2)	$MgH_{2-x}F_x$	3(1)	4.53(1)	3.04(1)
(MgF_2)				MgF_2	6(1)	4.60(1)	3.05(1)
Fe	8(1)	2.869(2)		Fe	3(1)	2.870(2)	
Fe(Mg)	3(1)	2.99(1)		Fe(Mg)	2(1)	2.984(3)	
(c) – hydrogenated				(f) – hydrogenated			
β-MgH_2	98(4)	4.518(1)	3.022(1)	β-MgH_2	93(1)	4.522(1)	3.023(1)
Fe	2(1)	2.868(2)		γ-MgH_2	1(1)	4.54(5)	4.96(4)
						5.41(4)	
				Mg	2(1)	3.21(1)	5.22(1)
				Mg_2FeH_6	4(1)	6.47(1)	
				Fe	1(1)	2.87(1)	

Mössbauer spectra were obtained by means of the MsAa-3 spectrometer with the commercial $^{57}Co(Rh)$ source kept at room temperature. Absorbers were kept at room temperature, too. Sample containing the highest amount of Mg_2FeH_6 was additionally measured at 4.2 K and afterwards at room temperature. Data were processed within transmission integral approximation as implemented in the MOSGRAF suite. All shifts are reported versus room temperature α-Fe.

3. Results

X-ray diffraction patterns are shown in Fig. 1, while resulting crystallographic parameters and particular compound abundances are listed in Table 1A. For the convenience of the phase identification Table 1B summarizes lattice parameters taken from the literature for relevant pure compounds. The as milled material doped with FeF_2 contains as the principal phase tetragonal β-MgH_2, quite significant amount of high pressure metastable orthorhombic γ-MgH_2 and some BCC iron having somewhat larger lattice constant than pure α-Fe probably due to formation of diluted Mg solid solution in iron. On the other hand, the as milled material doped with FeF_3 contains even more β-MgH_2 and a comparable amount of γ-MgH_2. Orthorhombic γ-MgH_2 is formed at about 8 GPa [6] and hence, appears commonly during milling of MgH_2. There is no crystalline iron as reported previously, but instead one can see a small amount of Mg_2FeH_6 [7–10].

Table 1B
Lattice constants taken from the literature for pure compounds corresponding to phases of the Table 1A.

	Space group	*a*, *b* (Å)	*c* (Å)
β-MgH_2	$P4_2/mnm$	4.517	3.021
γ-MgH_2	*Pbcn*	4.526	4.936
		5.448	
MgF_2	$P4_2/mnm$	4.625	3.052
Mg	$P6_3/mmc$	3.209	5.211
Mg_2FeH_6	$Fm3m$	6.443	
Fe	$Im3m$	2.867	

These results cannot be treated as quite certain as diffraction peaks are very broad and there is significant contribution from amorphous phase(s). All phases contain a lot of defects due to milling.

Dehydrogenation leads in both cases of FeF_2 and FeF_3 dopants to the formation of Mg as the dominant phase, a mixture of MgF_2 and $MgH_{2-x}F_x$ isostructural tetragonal phases and a mixture of BCC iron and isostructural solid solution of magnesium in iron. Dehydrogenation removes majority of defects and leads to highly ordered structures as seen by the small continuous background under diffraction pattern.

Table 2
Results obtained by Mössbauer spectroscopy at room temperature. The symbol *A* stands for contribution of the respective sub-profile (phase) to the total absorption profile, and symbol *S* denotes total shift versus room temperature α-Fe. The symbol Δ stands for splitting of the quadrupole doublet, while the symbol *B* denotes magnetic field leading to splitting into sextet. The symbol Γ stands for the absorber line-width. Marks (a)–(c) represent results for the FeF_2 doped material upon milling, dehydrogenation and hydrogenation, respectively. Marks (d)–(f) show corresponding results for the FeF_3 doped material. The average field <*B*> is shown for partly hydrated FeF_3 sample.

A (%)	*S* (mm/s)	Δ (mm/s) or *B* (T)	Γ (mm/s)	*A* (%)	*S* (mm/s)	Δ (mm/s) or *B* (T)	Γ (mm/s)
FeF_2				FeF_3			
91(1)	1.347(1)	Δ 2.767(2)	0.33(1)	94(2)	0.483(2)	<*B*> 37.9(1)	0.48(2)
9	0.52(1)	Δ 0.46(2)	0.31(3)	6	0.42(1)	Δ 0.65(1)	0.31(5)
(a) – FeF_2 doped: milled				(d) – FeF_3 doped: milled			
19(2)	−0.11(1)		0.32(2)	56(3)	−0.07(1)		0.38(1)
29	0.22(3)	Δ 0.56(4)	0.73(4)	27	0.43(3)	Δ 0.37(2)	0.47(4)
52(1)	−0.04(1)	*B* 31.3(1)	0.82(3)	17(1)	−0.03(2)	*B* 31.6(1)	0.48(8)
(b) – dehydrogenated				(e) – dehydrogenated			
5(1)	−0.02(1)		0.22(3)	35(3)	−0.09(2)		0.71(4)
40	0.30(1)	Δ 0.82(1)	0.71(2)	13	0.58(8)	Δ 0.34(9)	0.75(5)
55(1)	0.00(1)	*B* 32.94(1)	0.23(1)	52(1)	0.01(1)	*B* 32.2(1)	0.65(3)
(c) – hydrogenated				(f) – hydrogenated			
20(1)	−0.07(1)		0.32(2)	74(3)	−0.026(3)		0.32(1)
15	0.24(4)	Δ 0.91(6)	0.73(4)	10	0.36(7)	Δ 0.37(7)	0.36(9)
65(1)	0.00(1)	*B* 32.81(2)	0.35(1)	16(2)	0.05(3)	*B* 32.7(2)	0.40(9)

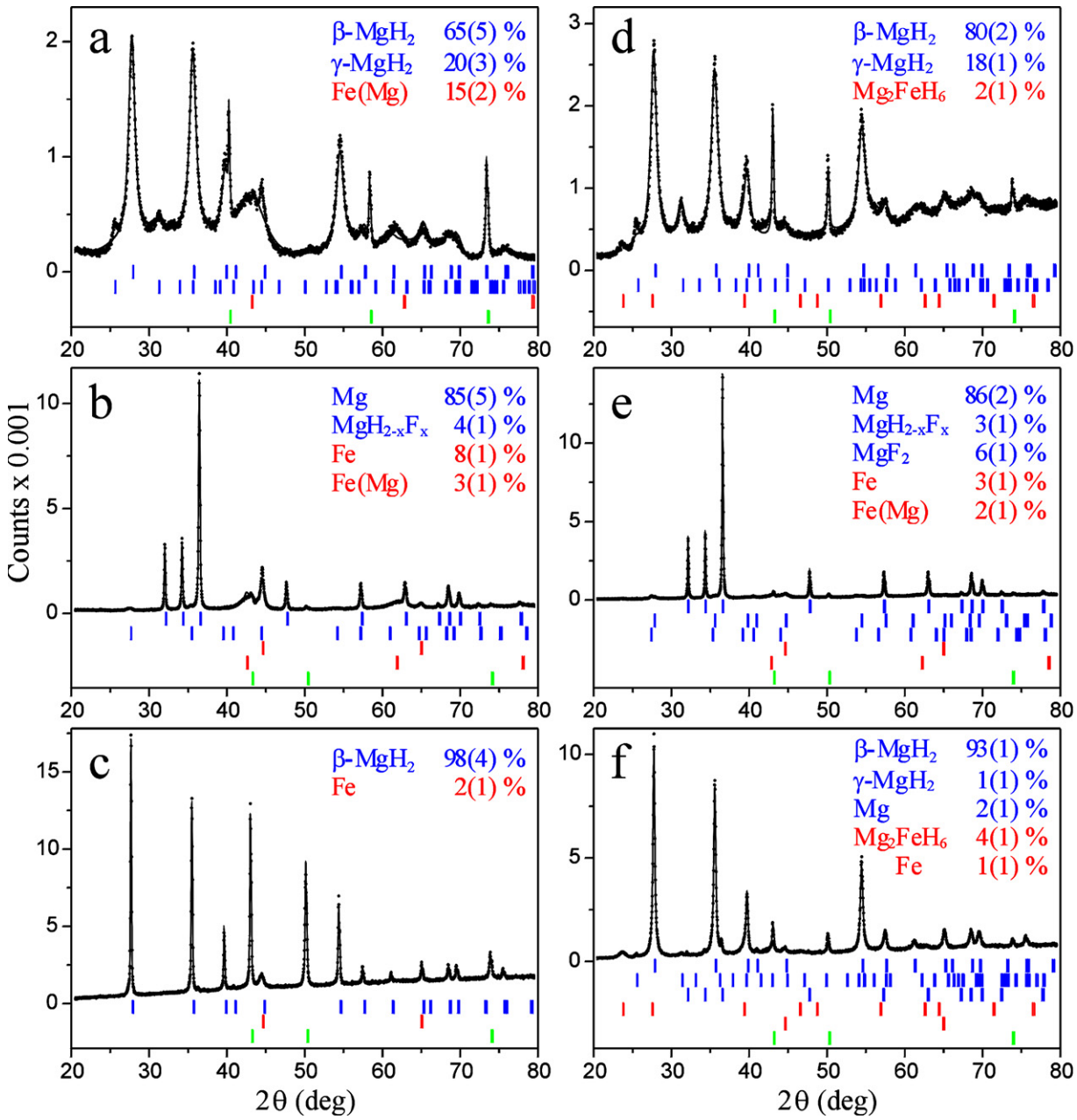

Fig. 1. Powder X-ray diffraction patterns versus scattering angle 2θ obtained with the Cu-Kα1, 2 radiation. Figures (a–c) show patterns for the FeF_2 doped material upon milling, dehydrogenation and hydrogenation, respectively. Figures (d–f) show corresponding patterns for the FeF_3 doped material. Bar diagrams have the same order as lists of recognized phases with abundances in wt.%. Diagrams shown in green are due to peaks of the sample container: Mo – (a), Cu – remaining patterns. (For interpretation of the references to color in this figure legend, the reader is referred to the web version of the article.)

Subsequent hydrogenation leaves β-MgH_2 with some small amount of the almost pure α-Fe in the case of FeF_2 dopant. For FeF_3 dopant β-MgH_2 is a dominant phase, too. However, one can see traces of γ-MgH_2, magnesium metal, α-Fe and relatively significant amount of Mg_2FeH_6 considering total iron content. Hence, one can conclude that metastable γ-MgH_2 is able to survive heating to moderate temperatures once formed. Similar behavior was observed by Lillo-Ródenas et al. [11]. Moreover hydrogenation increases material disorder, as the background in the diffraction pattern is larger than for the previous case.

X-ray diffraction is able, in principle, to see all phases having crystallographic order, while the Mössbauer spectroscopy recognizes all phases containing iron – either in the crystalline form or amorphous. Phases bearing iron are minor phases in this system due to the low iron concentration and hence, only the most abundant crystalline iron phases are distinguishable by the X-ray diffraction.

Room temperature Mössbauer spectra are shown in Fig. 2, while essential results are gathered in Table 2. Spectra were collected for both dopants (FeF_2 and FeF_3), as milled materials, and materials after dehydrogenation and subsequent hydrogenation. Ferrous fluoride is slightly contaminated by some highly disordered oxide containing ferric ions in the high-spin state. Strongest lines are due to the ferrous ion in the high-spin state exhibiting large quadrupole splitting and large isomer shift. Ferric fluoride is contaminated by similar oxide, albeit much better ordered. Additionally, it exhibits some degree of hydration [12].

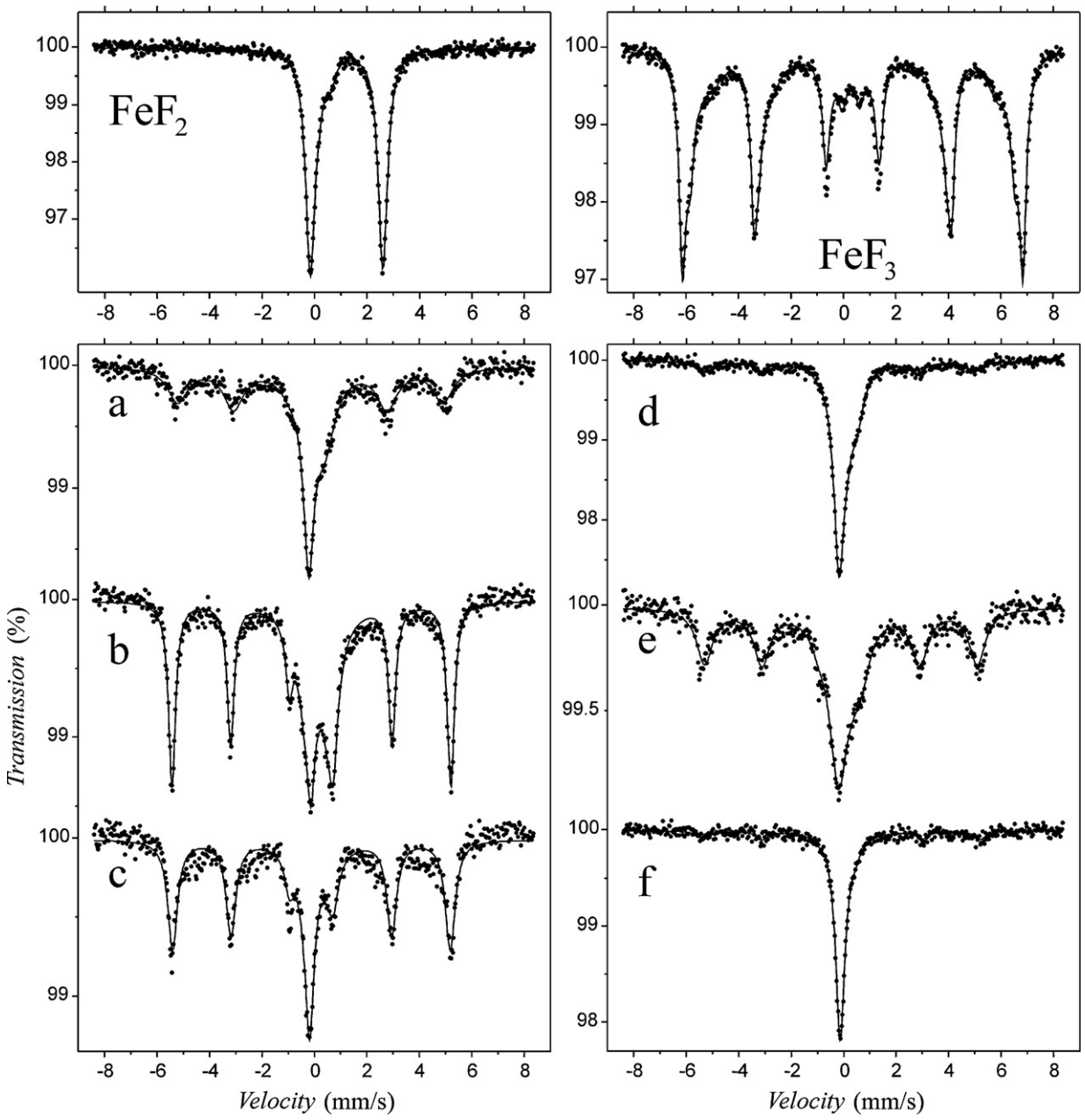

Fig. 2. Room temperature Mössbauer spectra. Figures (a–c) show spectra for the FeF_2 doped material upon milling, dehydrogenation and hydrogenation, respectively. Figures (d–f) show corresponding spectra for the FeF_3 doped material. Spectra of the respective materials used as dopants (FeF_2 and FeF_3) are shown as well.

The major part of the spectrum is due to the high-spin ferric ion and the compound is magnetically ordered at room temperature.

Milled, dehydrogenated and hydrogenated material is characterized by the presence of a singlet, quadrupole split doublet and magnetically split sextet for both dopants. Original iron fluorides disappear completely during milling and are never seen again. Singlet originates in the diamagnetic insulator Mg_2FeH_6 containing octahedrally coordinated low-spin divalent iron [7,13]. Doublet originates in the amorphous magnesium–iron alloy [14]. Sextet is due to BCC metallic iron. This iron contains dissolved magnesium upon milling, and is almost pure upon hydrogenation and subsequent dehydrogenation. Mg_2FeH_6 is produced during milling phase – much more efficiently with FeF_3 dopant in comparison with the FeF_2 dopant. Dehydrogenation leads to decrease of this compound abundance. The compound is restored upon subsequent hydrogenation.

Fig. 3 shows spectrum obtained at 4.2 K for the hydrogenated material being previously milled with FeF_3 dopant and subsequently dehydrogenated. Additional spectrum is shown for the same sample reheated to the room temperature. One can see that Mg_2FeH_6 does not order magnetically at very low temperatures confirming the low-spin state of divalent iron [7]. Furthermore doublet originating in the amorphous magnesium–iron alloy disappears due to the magnetic ordering of this minor phase at low temperature [14]. Reheated sample has the same spectrum as prior to cooling.

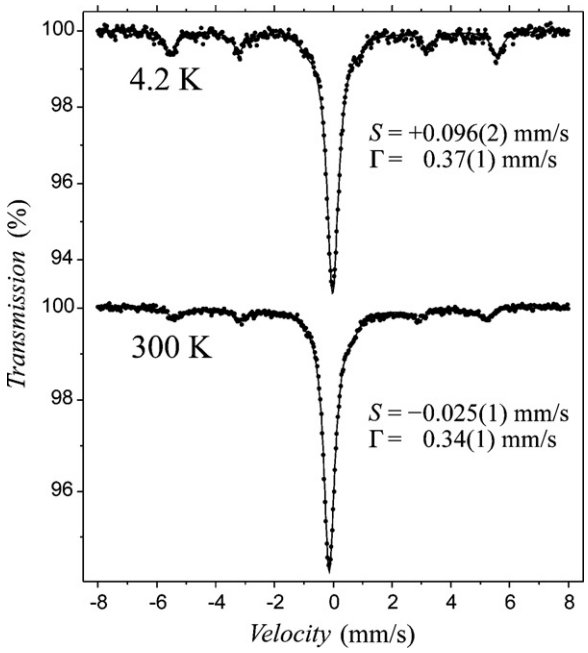

Fig. 3. Mössbauer spectrum of the hydrogenated material (previously milled and dehydrogenated) with FeF_3 dopant obtained at 4.2 K and at room temperature upon re-heating. Singlet is due to the Mg_2FeH_6 compound. The shift S and line-width Γ of the singlet are shown.

4. Conclusions

It seems that lower temperatures of hydrogenation and dehydrogenation of the magnesium are obtained in the presence of metallic Fe due to the strong catalytic properties of the 3d metal surface – particularly Fe. Hydrogen molecules have much lower dissociation energy on the contact with the iron surface – 3d electrons. Small iron particles having large active surface are obtained upon decomposition of fluorides.

It has been confirmed that Mg_2FeH_6 is produced during mechanical milling of magnesium hydride with iron fluoride dopants. Ferric fluoride is more efficient in making Mg_2FeH_6 than ferrous fluoride.

It has been confirmed that Fe occurs in the low-spin divalent state in Mg_2FeH_6 and hence, above compound is diamagnetic.

Acknowledgments

We are grateful to Prof. R.A. Varin from the University of Waterloo, Canada, for fruitful discussions. Materials investigated were synthesized within the Key Project POIG.01.03.01-14-016/08 of the Polish Ministry of Sciences and Higher Education.

References

[1] J.F.R. de Castro, A.R. Yavari, A. LeMoulec, T.T. Ishikawa, W.J. Botta, J. Alloys Compd. 389 (2005) 270.
[2] A.R. Yavari, A. LeMoulec, J.F.R. de Castro, S. Deledda, O. Friedrichs, W.J. Botta, G. Vaughan, T. Klassen, A. Fernandez, Å. Kvick, Scripta Mater. 52 (2005) 719.
[3] S.-A. Jin, J.-H. Shim, Y.W. Cho, K.-W. Yi, J. Power Sources 172 (2007) 859.
[4] I.E. Malka, T. Czujko, J. Bystrzycki, Int. J. Hydrogen Energy 35 (2010) 1706.
[5] I.E. Malka, J. Bystrzycki, T. Płociński, T. Czujko, J. Alloys Compd., doi:10.1016/j.jallcom.2010.10.122.
[6] J. Huot, G. Liang, S. Boily, A. Van Neste, R. Schulz, J. Alloys Compd. 293–295 (1999) 495.
[7] J.-J. Didisheim, P. Zolliker, K. Yvon, P. Fischer, J. Schefer, M. Gubelmann, A.F. Williams, Inorg. Chem. 32 (1984) 1953.
[8] P. Selvam, K. Yvon, Int. J. Hydrogen Energy 16 (1991) 615.
[9] J. Huot, S. Boily, E. Akiba, R. Schulz, J. Alloys Compd. 280 (1998) 306.
[10] A. Vaichere, D.R. Leiva, T.T. Ishikawa, W.J. Botta, Mater. Sci. Forum 570 (2008) 39.
[11] M.A. Lillo-Ródenas, Z.X. Guo, K.F. Aguey-Zinsou, D. Cazorla-Amorós, A. Linares-Solano, Carbon 46 (2008) 126.
[12] D.G. Karraker, P.K. Smith, Inorg. Chem. 31 (1992) 1118.
[13] L.A. Baum, M. Meyer, Z. Mendoza, Hyperfine Interact. 179 (2007) 61.
[14] A.M. van der Kraan, K.H.J. Buschow, Phys. Rev. B 25 (1982) 3311.